233

Radial cracking with closure

J.P. DEMPSEY[1], L.I. SLEPYAN[2] and I.I. SHEKHTMAN[1]
[1]*Department of Civil and Environmental Engineering, Clarkson University, Potsdam, New York 13699-5710, USA*
[2]*Department of Solid Mechanics, Materials and Structures,Tel Aviv University, Ramat Aviv 69978, Tel Aviv, Israel*

Abstract. Progressive radial cracking of a clamped plate subjected to crack-face closure is studied. The material behavior is assumed to be elastic-brittle. The cracks are assumed to be relatively long in the sense that the three-dimensional contact problem can be described via a statically equivalent two-dimensional idealization. The number of cracks is supposed large enough to permit a quasi-continuum approach rather than one involving the discussion of discrete sectors. The formulation incorporates the action of both bending and stretching as well as closure effects of the radial crack face contact. Fracture mechanics is used to explore the load-carrying capacity and the importance of the role of the crack-surface-interaction. For a given crack radius, the closure contact width is assumed to be constant. Under this condition, a closed-form solution is obtained for the case of a finite clamped plate subjected to a concentrated force. Crack growth stability considerations predict that the system of radial cracks will initiate and grow unstably over a significant portion of the plate radius. The closure stress distribution is determined exactly in the case of narrow contact widths and approximately otherwise.

1. Introduction

One of the major difficulties in the analysis of either the bearing capacity or penetration of an ice sheet [1, 2] is the treatment of the radial cracking that occurs (Fig. 1). The deformation of the wedge sectors, which are generated by the radial cracks at a load that is significantly below the breakthrough load, produces a wedging action [3] that closes the radial crack faces on the compressive side of the plate. To date, the coupled plane-bending interaction of the radial crack faces has been ignored [4, 5]. Historically, the difficulties introduced by such crack closure phenomena have long been recognized [6, 7, 8]; however, a framework for the application of fracture mechanics to cracked plates subjected to closure does not yet exist.

The objective of this paper is to provide such a framework. With this in mind, the fluid support is but an unnecessary complication. Further, the authors sought to analyze a problem that could be examined experimentally as well as theoretically. Therefore, the specific geometry chosen is that of a finite clamped plate subjected to a lateral central concentrated load. The key to the formulation is an adequate description of the coupling between the in-plane (u, S_r, S_θ) and out-of-plane (w, M_r, M_θ, Q_r) quantities. The extent of closure (the closure width) is assumed to be constant for a given cracked radius R. An analytical solution is provided for the crack closure problem under consideration in terms of the closure parameters that effectively couple the global planar and bending deformations of the thin plate.

The crux of the analysis presented in this paper is a rigorous specification of the closure parameters. The 'inner' or 'local' elasticity contact deformations in the vicinity of each crack closure region must be kinematically compatible with the 'outer' or 'global' plane-bending plate deformations. The formulation of the inner problem required that wide-ranging stress-intensity-factor and crack-opening-displacement expressions be provided for the edge-
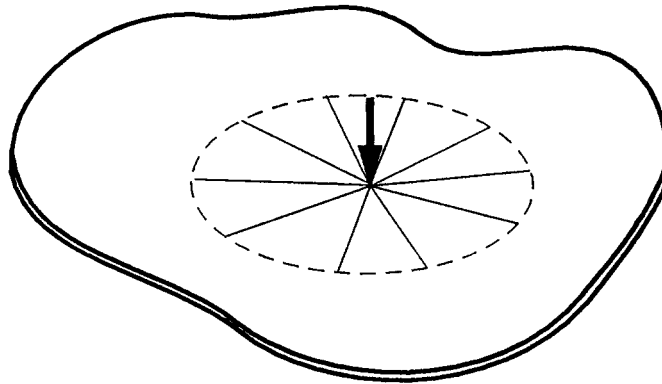
Fig. 1. A radially cracked plate.

cracked strip subjected to both an axial force and a moment; the latter problem was studied in some detail by Rice and Levy [9] in pursuit of surface crack solutions. While the energy balance may be deduced from either local or global considerations, the derivation of the local energy-release-rate expression proved to be non-traditional. The analytical solution noted above facilitated not only the verification of the final local expression but also an analytical expression for the energy-release-rate from the assumed pseudo-axisymmetric array of radial cracks.

A thorough examination of various aspects of the solution is included in this paper. The authors are pursuing, also, an experimental investigation of the cracking behavior associated with the lateral loading of a finite clamped semi-brittle plate.

2. Problem description

The progressive radial cracking of a finite clamped plate subjected to crack-face closure is now investigated. The material behavior is taken to be elastic-brittle. The cracks are assumed to be 'relatively' long in the sense that the three-dimensional contact problem can be described in a statically equivalent two-dimensional idealization. The viewpoint adopted in this paper forms one extreme in which one supposes that the large number of cracks formed permits a quasi-continuum axisymmetric approach rather than one involving the discussion of discrete sectors [8]. This supposition requires a formulation in which the interconnected action of both bending and stretching is treated as well as closure effects of the radial crack face contact. At the other extreme, it is necessary to model the deformation of a plate weakened by the presence of a few intersecting cracks only (the latter study is to be reported in a separate paper).

Consider, briefly, vertical loading under a downward concentrated load: under increasing loads, a surface crack would initiate at the bottom of the plate. This crack would then propagate up through-the-thickness as well as radially. At some juncture, further cracking would ensue such that eventually a multiply-radially-cracked zone has been developed. This paper assumes at the outset that such a zone has developed. Ultimately, in the present scenario, circumferential cracking would be caused by tension on the top surface of the plate.

The crack face interaction that occurs after a number of radial cracks have 'popped in' produces a wedging action that allows the plate to carry an additional load (until circumferential cracking or penetration occurs). This wedging action, or crack face interaction, should

be more evident for thicker sheets. Actually, the crack face interaction is a complicated three-dimensional contact problem. The contact pressure distribution is unknown and acts over an unknown area. The constraint that the contact pressure be positive (compressive) or zero, thus excluding tensile tractions on the crack faces, in itself makes the problem nonlinear (even for small deformations and linearly elastic material behavior). In this paper, the contact strip width, as well as the closure stress distribution, is determined. The influence of the number of cracks is included in these calculations.

The classification of the closure contact situation (in the through-the-thickness direction) of the radial crack faces leads directly to several important generalizations. Since the contact is of the 'receding' type [10], the contact area changes discontinuously from its initial to its loaded extent and shape on application of the first increment of load. Further, if the nature of the loading does not change but increases in magnitude only, and if the cracked zone radius does not change, the extent and shape of the closure contact does not change. The final special property of receding contacts is especially important in the context of the problem under consideration in this paper: the intensity of the closure stress distribution will increase, without change in form, in direct proportion to the load.

The general problem under consideration is based on both the coupled plane-bending problem as well as the plane crack closure problem. The first sub-problem is viewed as an axisymmetric multi-sectored quasi-continuum thin plate problem. The latter is an elasticity problem which induces an additional self-equilibrated stress distribution on the crack surfaces. The 'inner' contact problem is matched to the 'outer' plate problem by matching the 'outer' circumferential extension and rotation (quantities that can be expressed in terms of certain averaged integrals of the inner crack opening displacement) with the kinematic (Kirchhoff–Poisson) requirement that planes remain plane and normal to the neutral axis. The latter kinematic condition is imposed over a horizontal 'plane' at $z = e_c$ in the cracked zone ($0 \leqslant r \leqslant R, 0 \leqslant \theta \leqslant 2\pi$) on which the plate is considered to be rigid. In other words the axisymmetric 'zero circumferential displacement condition' is imposed only at one z value. Note that the associated value of e_c depends on the cracked zone radius R. An additional kinematic condition is specified to ensure rotational compatibility along the θ-lines bisecting each wedge sector formed by the n radial cracks. The parameters e_f (see Fig. 2c) and e_c may be looked upon as 'outer' or remote loading and kinematic variables, respectively, while the crack length a in the thickness direction is the inner contact variable. It is especially important to note that the closed form solution is derived assuming e_f and e_c to be constant for a given cracked zone of radius R. The strength of the formulation then resides in the fact that e_f and e_c can (and do) vary with each and every radius R.

The solution development incorporates two areas: the crack closure area and the intact area. Discontinuities or 'jumps' in M_θ and S_θ at the closure-intact interface produce the total energy release rate; the expression for the latter is derived by taking a variation of the crack closure area. This energy release is assumed to be uniformly distributed amongst a finite number of cracks. The latter number is assumed to be specified. In the following, the complete formulation of the problem is given. Different factors considered include the merits of a solution with a central hole (which at first sight might appear to be simpler) and the energy release rate obtained by the quasi-continuum formulation.
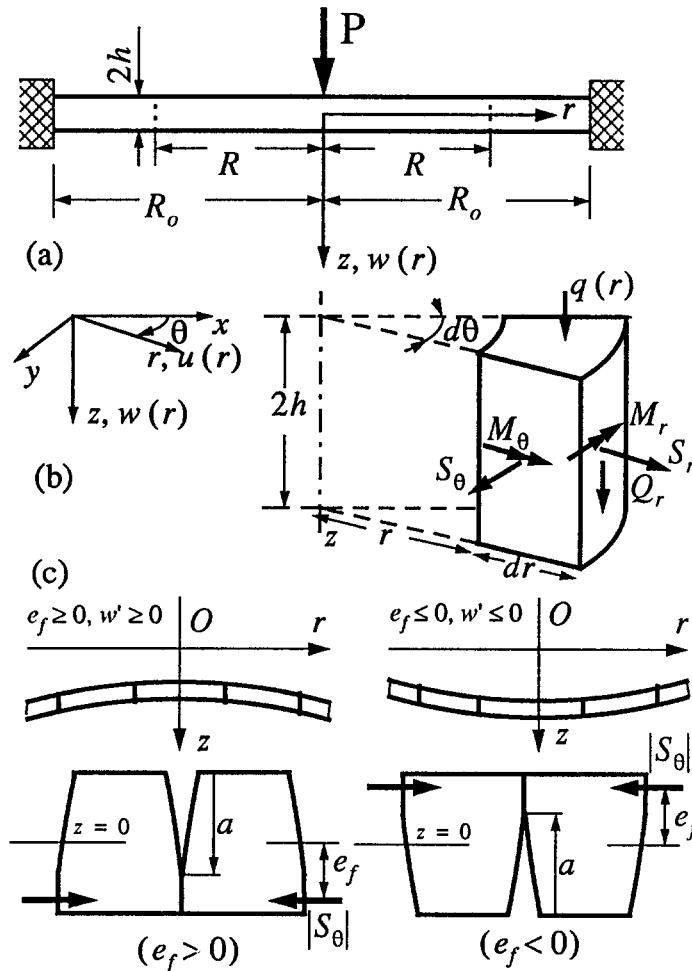
Fig. 2. A radially cracked clamped circular plate loaded by a central concentrated force: (a) plate configuration and dimensions; (b) coordinates and sign convention; (c) two closure scenarios and definition of e_f.

3. Formulation

The quantities $w(r)$ and $u(r)$ denote the vertical and radial displacements of the plate in the central plane ($z = 0$) respectively, and $u_r(r, z)$ is the radial displacement for arbitrary $z(u(r) \equiv u_r(r, 0))$

$$u_r(r, z) = u(r) - zw'(r), \tag{1}$$

Note that $w' \equiv \mathrm{d}w/\,\mathrm{d}r$. S_r and S_θ denote the in-plane radial and tangential forces, respectively, per unit length and M_r and M_θ denote the radial and tangential bending moments. In addition, let Q_r denote the radial shear force per unit length. In the equations to follow, E, ν, ρ, h denote the plate's Young's modulus, Poisson's ratio, density and half-thickness, respectively.

The radially cracked plate configuration (Fig. 1) is separated into the following regimes (Fig. 2a): the crack closure area (the inner region $r < R$), and the unbroken or intact plate (the outer region, $R < r < R_o$). The cracks are assumed to be uniformly distributed for $r < R$. The in-plane interaction force S_θ is compressive in the crack closure area. The formulation

here prescribes that S_θ acts at $z = 0$. In addition to this in-plane force, a moment M_θ acts at the same radial location on $\theta = $ constant. This force and moment are statically equivalent to the force S_θ acting at $z = e_f$ (Fig. 2c). The latter force is statically equivalent to the crack closure forces acting within the crack closure regime. The plate closure parameter e_f caused by the wedging action can occur either below or above the neutral axis, depending on whether the plate is subjected to uplift $(w' \geqslant 0)$ or is being pushed down $(w' \leqslant 0)$, respectively. In other words,

$$e_f \geqslant 0 \text{ if } w' \geqslant 0 \quad \text{and} \quad e_f \leqslant 0 \text{ if } w' \leqslant 0. \tag{2}$$

In the general case $e_f \neq 0$, and the force S_θ causes a bending moment M_θ; the occurrence of this in-plane force S_θ thus couples the planar and bending deformations.

At any point in the plate (in either region) the equations of equilibrium are given by

$$S_\theta = (rS_r)', \quad M_\theta = (rM_r)' + rQ_r, \quad (rQ_r)' = 0. \tag{3}$$

In addition, in both regimes,

$$EIw'' = M_r - \nu M_\theta, \quad 2Eh u' = S_r - \nu S_\theta. \tag{4}$$

In (4a), $I = 2h^3/3$.

In the intact or uncracked region $(R < r \leqslant R_o)$, the deflection of a thin circular plate must satisfy

$$\Delta^2 w = 0, \quad \Delta = \frac{1}{r}\frac{\mathrm{d}}{\mathrm{d}r}(r\frac{\mathrm{d}}{\mathrm{d}r}). \tag{5}$$

In addition, the following definitions for the moments, shear force and tangential strain are applicable in the uncracked regime only

$$\begin{aligned}
M_r &= D(w'' + \nu w'/r), \quad M_\theta = D(w'/r + \nu w''), \\
Q_r &= -D(w'' + w'/r)', \quad 2Eh\, u/r = S_\theta - \nu S_r,
\end{aligned} \tag{6}$$

where $D = E'I$; $E' = E/(1 - \nu^2)$.

Finite clamped plate. In this paper, the plate is assumed to be clamped at $r = R_o$, with the boundary conditions

$$w(R_o) = 0, \quad w'(R_o) = 0, \quad u(R_o) = 0. \tag{7}$$

The clamped plate is assumed to be subjected to a vertical concentrated load at the center; no concentrated radial actions are applied. That is,

$$2\pi r Q_r = -P, \quad \lim_{r \to 0} r M_r = 0, \quad \lim_{r \to 0} r S_r = 0. \tag{8}$$

For reference purposes, the solution for a finite uncracked clamped plate subjected to a central concentrated load is stated here (Timoshenko and Woinowsky–Krieger, [11]):

$$\begin{aligned}
w(r) &= P\left(R_o^2 - r^2 + 2r^2 \ln(r/R_o)\right)/16\pi D, \\
M_r(r) &= P\left((1 + \nu)\ln(r/R_o) + 1\right)/4\pi \\
M_\theta(r) &= P\left((1 + \nu)\ln(r/R_o) + \nu\right)/4\pi \\
Q_r(r) &= -P/2\pi r
\end{aligned} \tag{9}$$

In addition, in an uncracked finite clamped plate, under the conditions considered,

$$u(r) = 0, \quad S_r(r) = 0, \quad S_\theta(r) = 0, \quad (0 \leqslant r \leqslant R_o). \tag{10}$$

Note that the central displacement of the intact plate is given by

$$w(0) = w_o = PR_o^2/16\pi D. \tag{11}$$

Localized loading. The expressions $(9)_2$ and $(9)_3$ are logarithmically singular in r as r approaches zero and do not realistically portray the bending moments near the plate center. In addition, the underlying assumptions of the elementary theory of bending of circular plates do not hold near the point of application of a concentrated load. Suppose a load P is uniformly distributed over a circle of radius c and applied at the plate center on the surface $(z = -h)$. As c decreases, $\sigma_z = -P/\pi c^2$ increases rapidly; for small c, σ_z cannot be neglected in comparison with the bending stresses as is done in the elementary theory. Timoshenko and Woinowsky–Krieger [11] (Article 19) provide a lengthy discussion of this topic; here just the main points are noted.

The maximum tensile stress at the center of a clamped plate at the lower surface $(z = h)$ as $c \to 0$ is given by

$$(\sigma_r)_{\max} = (\sigma_\theta)_{\max} = P(1 + \nu) \left(0.485 \ln(R_o/2h) + 0.52 \right) / 4h^2. \tag{12}$$

The compressive strength of a quasi-brittle material is usually many times greater than its tensile strength; the compressive stresses $(\sigma_r, \sigma_\theta$ and $\sigma_z)$ at the top surface are highly localized. If the radius c of loading is small, but large enough to preclude significant crushing in the contact zone or failure due to shear and consequent punch through, the expression in (12) can be used to predict the load at incipient radial cracking of the intact plate.

'Hole' versus 'non-hole' formulation. At first glance it may seem appealing to re-formulate the problem and include a 'hole' of 'small' radius r_o at the plate center. Moreover, this approach is clearly valid if the solution is mainly independent of this small parameter r_o. However, a new problem arises: there is no information concerning the 'effective' or valid value of the hole radius r_o. Fortunately, if the solution is mainly independent of this small parameter, the hole radius can be taken to be zero without an essential change in the solution. For instance, consider the local conditions in the case of a plate loaded solely by a concentrated load P. With no concentrated radial actions applied the conditions at the plate center are as stated in (8). The 'hole solution' satisfies these requirements if its radius $r_o \to 0$. The question is what is the difference between these two solutions for $r > r_o$.

For a linear problem, the difference between the hole solution $(r_o > 0)$ and non-hole solution $(r_o = 0)$ is caused by the loading at $r = r_o$, viz.,

$$Q_r = 0, \quad S_r = -S_r^o, \quad M_r = -M_r^o \quad (r = r_o). \tag{13}$$

where S_r^o and M_r^o correspond to the non-hole solution. The work of these quantities is $O((S_r^{o2} + M_r^{o2})r_o)$. However, each quantity is logarithmically singular in r and hence the work tends to zero as $r_o \to 0$. It follows that the difference between the hole and non-hole solutions for $r \gg r_o$ will be negligible if r_o is small enough.

The hole solution augments the non-hole solution solely with the appearance of a boundary layer variation existing only within a distance of several r_o. The non-hole solution is preferable

Table 1. Energy-release ratios

n	G_n/G_∞	n	G_n/G_∞
2	0.810570	6	0.998242
3	0.967697	7	0.999064
4	0.990541	8	0.999456
5	0.996274	9	0.999662

because it is simpler, it is independent of unknown conditions at the plate center, and it is the same as the hole solution outside of the boundary layer type near hole region.

'Few' versus 'many' cracks. The viewpoint adopted in this paper forms one extreme in which one supposes that the large number of cracks formed permits a quasi-continuum axisymmetric approach rather than one involving the discussion of discrete sectors. Here it is shown that this approach is plausible, even for rather few cracks.

To this end, consider the plane star crack in an infinite elastic thin plate of thickness $t \equiv 2h$ with a central hole of a vanishingly small radius r_0 under the radial pressure $\sigma_r = -F/tr_0$. In this case, the force which acts at the vertex of each wedge in the star crack problem is given by $P_n = 2F\sin(\pi/n)$, where n is the number of the radial cracks. The number of cracks here is finite and no quasi-continuum axisymmetric assumption is required. The associated stress intensity factor is denoted here by K_n and is available from [13] (page 8.18); the total energy-release-rate is denoted by G_n and is given by

$$G_n = \frac{nK_n^2}{E} = \frac{4F^2n}{t^2ER}\sin^2\left(\frac{\pi}{n}\right)\left(\frac{2\pi}{n} + \sin\left(\frac{2\pi}{n}\right)\right)^{-1}, \tag{14}$$

where E is the elastic modulus and R is the length of each crack and the radius of the cracked zone.

Now consider the same problem but let there be a large enough number of cracks such that the quasi-continuum axisymmetric assumption is tenable. For the conditions considered, there are two regions. The first region is an open crack area where the radial displacement, u, and the radial stresses, σ_r are described by $u = -(F/tE)\ln r + C$, $\sigma_r = -F/tr$, where r is the radial coordinate, and C is a constant. The second region is the intact plane where $u = A/tEr$, $\sigma_r = -A/(1+\nu)tr^2$, where ν is the plate's Poisson's ratio, and A is another constant. The constants C and A can be found using the continuity conditions at $r = R$. The radial displacement is then found to be given by $u = -(F/tE)(\ln(r/R) - (1+\nu))$. The total energy-release-rate in this case is denoted by G_∞

$$G_\infty = \lim_{n\to\infty} G_n = \frac{1}{2}2\pi\frac{F}{t}\frac{\partial u}{\partial R} = \frac{\pi F^2}{t^2ER}. \tag{15}$$

The ratio $\mathcal{E}_n = G_n/G_\infty$ of the total energy release rate from the 'finite or few crack' case to the 'many crack' case turns out to be remarkably close to unity even for $n = 2$ (this is actually only one crack, and only in polar coordinates does it look as two cracks). For higher n (see Table 1) this ratio rapidly approaches unity (in fact, $1 - \mathcal{E}_n \sim \pi^4/(45n^4)$ as $n \to \infty$). This comparison reveals, at least in the case of plane crack problems, that the energy release

rate may well be rather insensitive with respect to the crack number. Moreover, the quasi-continuum model may estimate the energy release rate rather well, and hence also the radius of the cracked zone.

4. Radial cracking analysis

The crack closure parameters e_f and e_c introduced in this paper are assumed to be constant and not functions of radius r. These parameters are, however, assumed to be functions of crack radius R. That is,

$$e_f \equiv e_f|_R, \quad e_c \equiv e_c|_R. \tag{16}$$

Crack closure region ($0 \leqslant r \leqslant R$)**.** The tangential force exists only in the crack surface interaction area ($0 \leqslant r \leqslant R$), in which case

$$S_\theta \leqslant 0. \tag{17}$$

The key to the formulation is the coupling between the in-plane (u, S_r, S_θ) and out-of-plane (w, M_r, M_θ, Q_r) quantities (Fig. 2b). This plane-bending coupling occurs solely through the expressions for M_θ and ϵ_θ

$$M_\theta = -S_\theta e_f, \quad S_\theta \leqslant 0, \tag{18}$$

$$\epsilon_\theta = (u - e_c w')/r = (S_\theta - \nu S_r)/2Eh - e_c(M_\theta - \nu M_r)/EI, \tag{19}$$

where $I = 2h^3/3$.

The appropriate solution in this radially cracked region of the plate is deduced by expressing M_r and S_r each in the form 'constant' times $\ln(r/R)$ plus another 'constant'. Equations (3), (4), (13), (18) and (19) quickly yield, then, for the inner region ($0 \leqslant r \leqslant R$),

$$
\begin{aligned}
EIw(r) &= -e_f(1-\nu)r^2 S_r(r)/2 - e_f(3-\nu)\hat{S}_1 r^2/4, \\
&\quad +Pr^2/4\pi + C_3 r + C_4, \\
M_r(r) &= -e_f S_r(r) + P/2\pi, \\
M_\theta(r) &= -e_f S_\theta(r), \\
2Ehu(r) &= (1-\nu)r S_r(r) + \hat{S}_1 r + \gamma C_3/e_f, \\
S_r(r) &= -\hat{S}_1 \ln(r/R) + S_2, \\
S_\theta(r) &= -\hat{S}_1 \ln(r/R) + S_2 - \hat{S}_1,
\end{aligned}
\tag{20}
$$

in which C_3, C_4 and S_2 are unknown constants and

$$\hat{S}_1 = \left(\frac{P}{2\pi}\right) \frac{(1+\nu)\gamma}{2e_f(1+\gamma)}, \quad \gamma = e_c e_f \frac{2Eh}{EI} = 3\left(\frac{e_c}{h}\right)\left(\frac{e_f}{h}\right). \tag{21}$$

Open crack region ($\rho_i \leqslant r/R \leqslant \rho_o$)**.** Suppose a portion of the inner radially cracked region experiences no crack surface interaction in the sub-region between $\rho_i R$ and $\rho_o R$; in this case,

$$M_\theta = 0, \quad S_\theta = 0 \quad (\rho_i \leqslant r/R \leqslant \rho_o). \tag{22}$$

In the above equation $\rho_i \geqslant 0$ and $\rho_o \leqslant 1$. Expressions for the in-plane and out-of-plane quantities in the inner radially cracked region are very much simpler if the crack region concerned is open (with no crack surface interaction). In an open crack region, therefore, the non-zero quantities are given by

$$
\begin{aligned}
EIw(r) &= Pr^2/4\pi + B_3 \left(r \ln(r/R) - r\right) + B_4 r + B_5, \\
M_r(r) &= P/2\pi + B_3/r, \\
u(r) &= B_1 \ln(r/R) + B_2, \\
S_r(r) &= 2EhB_1/r.
\end{aligned}
\tag{23}
$$

In the above equations, $B_j, j = 1, 2, \ldots 5$, are unknown constants.

Intact region $(R < r \leqslant R_o)$. It follows from (5), (6), (3a) and (4b) that in the intact or uncracked region $(R < r \leqslant R_o)$

$$
\begin{aligned}
w(r) &= d_1 r^2 \ln(r/R) + d_2 r^2 + d_3 \ln(r/R) + d_4, \\
M_r(r) &= D(2(1+\nu)d_1 \ln(r/R) + (3+\nu)d_1 \\
&\quad +2(1+\nu)d_2 - (1-\nu)d_3/r^2), \\
M_\theta(r) &= D(2(1+\nu)d_1 \ln(r/R) + (1+3\nu)d_1 \\
&\quad +2(1+\nu)d_2 + (1-\nu)d_3/r^2), \\
2Ehu(r) &= (1-\nu)d_5 r + (1+\nu)d_6/r, \\
S_r(r) &= d_5 - d_6/r^2, \\
S_\theta(r) &= d_5 + d_6/r^2.
\end{aligned}
\tag{24}
$$

In the above equations, $d_j, j = 1, 2, \ldots 6$ are unknown constants. The plate is clamped at $r = R_o$; the associated conditions stated in (7) and (8) imply that

$$
\begin{aligned}
d_1 &= P/8\pi D, \\
d_3/R_o^2 &= 2d_1 \ln \zeta - d_1 - 2d_2, \\
d_4/R_o^2 &= 2d_1 \ln^2 \zeta - (1 + 2\ln \zeta)d_2, \\
d_6/R_o^2 &= -b^2 d_5,
\end{aligned}
\tag{25}
$$

in which $\zeta = R/R_o$.

Continuity conditions at $r = R$. The general solutions given in (21), (24) and (25) contain many unknown constants which are determined by the continuity conditions operative at the contour separating the cracked regime from the uncracked regime. With the notation

$$
[J] \equiv J(R^+) - J(R^-) \equiv J^+ - J^-,
\tag{26}
$$

the static and kinematic conditions of continuity are

$$
\begin{aligned}
[S_r] &= 0, \quad [M_r] = 0, \quad [Q_r] = 0, \\
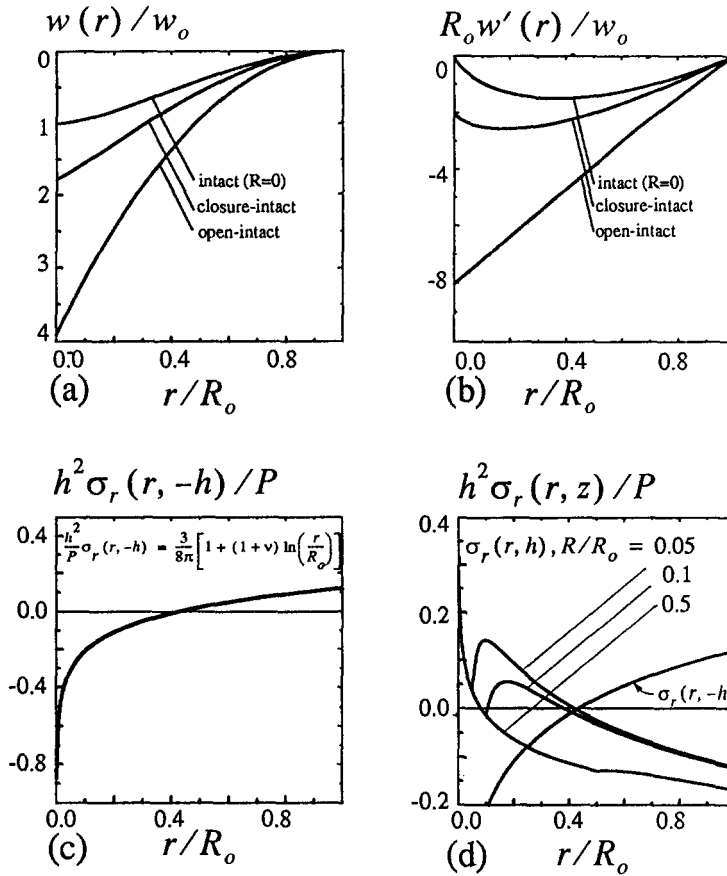[u] &= 0, \quad [w] = 0, \quad [w'] = 0.
\end{aligned}
\tag{27}
$$

Fig. 3. (a) Deflection $w(r)$, (b) slope $w'(r)$, (c) radial stresses $\sigma_r(r, -h)$, and (d) $\sigma_r(r, \pm h)$ plotted versus r/R_o for $\nu = 0.2, e_f = e_c = -h$, and $R/R_o = 0.5$.

These continuity conditions imply, on examining (3) and (4), that

$$[S_\theta] = R[S_r'], \quad [M_\theta] = R[M_r']$$

$$[u'] = -\frac{\nu}{2Eh}[S_\theta], \quad [w''] = -\frac{\nu}{EI}[M_\theta]. \tag{28}$$

In the case of crack closure, (19) and (27) imply that

$$[S_\theta] = \frac{\gamma}{e_f}[M_\theta]. \tag{29}$$

Closure-intact solution. The solution is presented here for the case in which the crack surfaces interact over the whole extent of the radially cracked zone ($0 \leqslant r \leqslant R$). The equations stated in (21), (25) and (26) are then subject to the continuity conditions stated in (27). The constants C_3, C_4, S_2, and $d_j, j = 1, 2, \ldots 6$ are now given by

$$(1 + \gamma)C_3 = PR\left(2\hat{C}_3 - (1 + \nu)\right)/4\pi,$$

$$(1 + \gamma)(C_4 - EIw_o) = PR^2\left((1 + \nu)^2 + 4\hat{C}_4\right)/16\pi,$$

$$e_f(1 + \gamma)S_2 = \gamma P\left(1 - (1 + \nu)\ln\zeta\right)/4\pi,$$

$$Dd_1 = P/8\pi,$$
$$4(1+\nu)Dd_2 = P/2\pi + C_3/R - e_f\hat{S}_1 - 2e_fS_2,$$
$$2(1-\nu)Dd_3/R^2 = (1+\nu)P/4\pi(1+\gamma) + C_3/R,$$
$$(1-\nu^2)Dd_4/R^2 = (1+\nu)P/8\pi(1+\gamma) + (3+\nu)C_3/4R + C_4/R^2,$$
$$(\zeta^2+b^2)d_5 = \zeta^2S_2,$$
$$(\zeta^2+b^2)d_6 = -R^2b^2S_2,$$

(30)

in which

$$b^2 = (1-\nu)/(1+\nu)$$
$$(\zeta^2+b^2)\hat{C}_3 = -b^2\left(1 - (1+\nu)\ln\zeta\right),$$
$$(\zeta^2+b^2)\hat{C}_4 = b^2\left(1 - (1+\nu)\ln\zeta\right)^2.$$

(31)

In $(30)_2$ note that w_o was defined earlier in (11).

The conditions in (28) give

$$[M_\theta] = \frac{P}{2\pi}\frac{1+\nu}{1+\gamma} + \frac{C_3}{R},$$

(32)

with $[S_\theta]$ given by (29).

The in-plane quantities S_r and S_θ are especially simple and will be presented here for later use. In the region $(0 \leqslant r \leqslant R)$,

$$e_f(1+\gamma)S_r = \gamma P\left(1 - (1+\nu)\ln(r/R_o)\right)/4\pi,$$
$$e_f(1+\gamma)S_\theta = -\gamma P\left(\nu + (1+\nu)\ln(r/R_o)\right)/4\pi,$$

(33)

while in the region $(R < r \leqslant R_o)$

$$(\zeta^2+b^2)S_r = \left(\zeta^2 + (R/r)^2b^2\right)S_2,$$
$$(\zeta^2+b^2)S_\theta = \left(\zeta^2 - (R/r)^2b^2\right)S_2.$$

(34)

An analytical expression for the central displacement of the plate is now readily obtained and is remarkably simple

$$EIw(0) = EIw_o + \frac{PR^2}{16\pi}\frac{(1+\nu)^2}{(1+\gamma)} + \frac{PR^2}{4\pi}\frac{b^2\left(1 - (1+\nu)\ln\zeta\right)^2}{(\zeta^2+b^2)(1+\gamma)}.$$

(35)

Open-intact solution. The solution presented here is for the case in which crack closure of the radial crack surfaces is *ignored* over the whole extent of the radially cracked zone $(0 \leqslant r \leqslant R)$. Crack interpenetration is presumed to occur without restraint. This solution is presented to examine the closure influence quantitatively. In this case, the equations stated in (24), (25) and (26) are subject to the continuity conditions stated in (27). It follows that

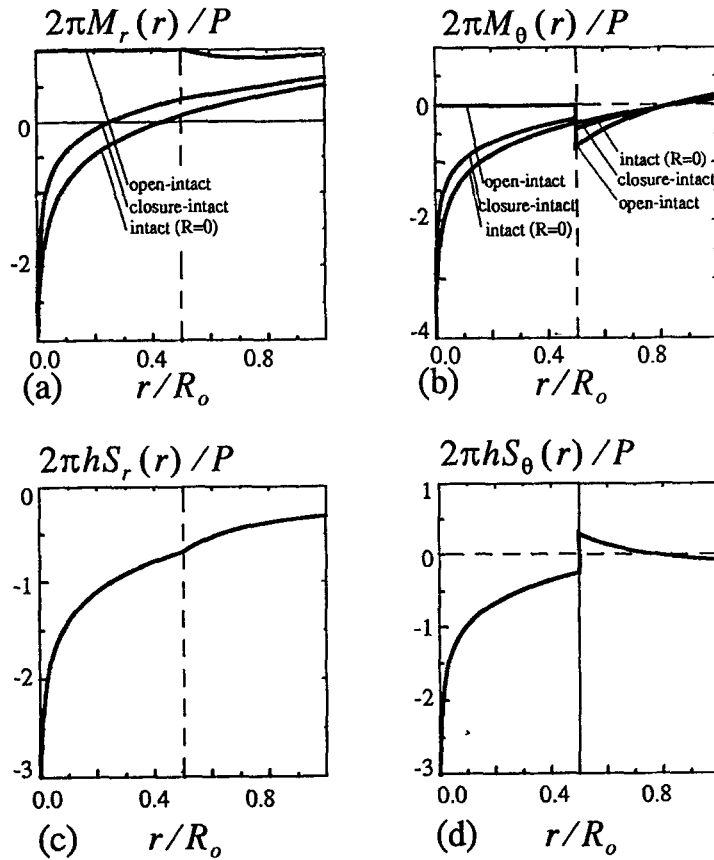$$B_1 = B_2 = B_3 = 0, \quad d_5 = d_6 = 0,$$

(36)

Fig. 4. (a) Radial bending moment $M(r)$, (b) tangential bending moment $M_\theta(r)$, (c) radial force $S_r(r)$, and (d) tangential force $S_\theta(r)$ plotted versus r/R_o for $\nu = 0.2$, $e_f = e_c = -h$, and $R/R_o = 0.5$.

and that

$$B_4 = (1 + \gamma)C_3,$$
$$(B_5 - EIw_o) = (1 + \gamma)(C_4 - EIw_o),$$
$$4(1 + \nu)Dd_2 = P/2\pi + B_4/R, \tag{37}$$
$$2(1 - \nu)Dd_3/R^2 = (1 + \nu)P/4\pi + B_4/R,$$
$$(1 - \nu^2)Dd_4/R^2 = (1 + \nu)P/8\pi + (3 + \nu)B_4/4R + B_5/R^2.$$

The conditions in (28) give

$$[M_\theta] = (1 + \nu)\frac{P}{2\pi} + \frac{B_4}{R}, \quad [S_\theta] = 0. \tag{38}$$

Closure-intact versus open-intact solution. Note that the jump in the tangential bending moment $[M_\theta(R)]$ (closure-intact) (32) differs from $[M_\theta(R)]$ (open-intact) (38) simply by the divisor $1 + \gamma$. This divisor reappears in the energy-release rate expression derived later in the paper. Moreover, given that $[S_\theta(R)]$ is related to $[M_\theta(R)]$ by (29) for closure, or $[S_\theta(R)]= 0$ for open regions, and given the form of the energy-release-rate G in (93), it is readily apparent that $G = 0$ when $[M_\theta]= 0$. Clearly, since the factor of $1 + \gamma$ is removable from $[M_\theta]= 0$,

Table 2. G = 0 or [$\dot{M}_\theta$]= 0

ν	ζ_c	ν	ζ_c
0.0	1.0000	0.3	0.7627
0.1	0.9088	1/3	0.7412
0.2	0.8312	0.4	0.6998
1/4	0.7961	0.5	0.6396

the radii R_c at which $G = 0$ are not influenced by closure effects. These radii are listed in Table 2 ($\zeta_c = R_c/R_o$) for various values of Poisson's ratio.

For illustrative purposes, several plots of the above closed-form solutions are provided. In Fig. 3(a-d), the (a) deflection $w(r)$, (b) slope $w'(r)$, and (c) radial stresses $\sigma_r(r, -h)$, and (d) $\sigma_r(r, \pm h)$ are plotted versus r/R_o given $\nu = 0.2$, $e_f = e_c = -h$, and $R/R_o = 0.5$. In Fig. 4(a-d), the (a) radial bending moment $M(r)$, (b) tangential bending moment $M_\theta(r)$, (c) radial force $S_r(r)$, and (d) tangential force $S_\theta(r)$ are plotted versus r/R_o given $\nu = 0.2$, $e_f = e_c = -h$, and $R/R_o = 0.5$. Note here that the assumption that $e_f = e_c = -h$ is an extremal case: later in the paper it becomes evident that this case implies that R_o/nh is very large and that the crack lengths are very large.

Figure 3a portrays the dramatic increase in stiffness brought about by the inclusion of the influence of closure as compared to an analysis ignoring crack closure and freely permitting crack-face interpenetration. The plot shows that disregarding closure may considerably underestimate the bending stiffness of the plate. In Fig. 3c and 3d, the radial stresses are defined by

$$\sigma_r(r, z) = \frac{S_r(r)}{2h} - \frac{z}{h}\frac{3M_r(r)}{2h^2}. \tag{39}$$

The expression for $\sigma_r(r, -h)$ in Fig. 3c, as indicated by the equation on the plot, is remarkable; within the problem formulation and boundary conditions considered this expression is evidently invariant with respect to the crack length R. The magnitude of $\sigma_r(r, -h)$ is directly proportional to P. It may, therefore, vary with the load, but the shape is universal. Expressions of this type need to be considered in order to evaluate the full failure sequence, from radial cracking to circumferential cracking and penetration.

5. Contact problem in the closure region

In the closure region ($0 \leqslant r \leqslant R$), the global planar and bending deformations of the thin plate are well described by the usual assumptions (for example, planes remain plane and perpendicular to the neutral axis). However, 'close' to each crack surface interaction area, the deformations can only be described by an 'inner' or 'local' elasticity solution. The stress distribution of the local problem differs from that for the global problem by a self-equilibrated stress field; the latter causes an additional crack opening displacement such that 'far enough' from each crack the actual physical extent of contact can be deduced only by prescribing kinematic compatibility.

Edge-cracked strip in tension and bending. Similar to the paper by Rice and Levy [9], the solution for an edge-cracked strip (Fig. 5) in plane strain subjected to an axial force S and
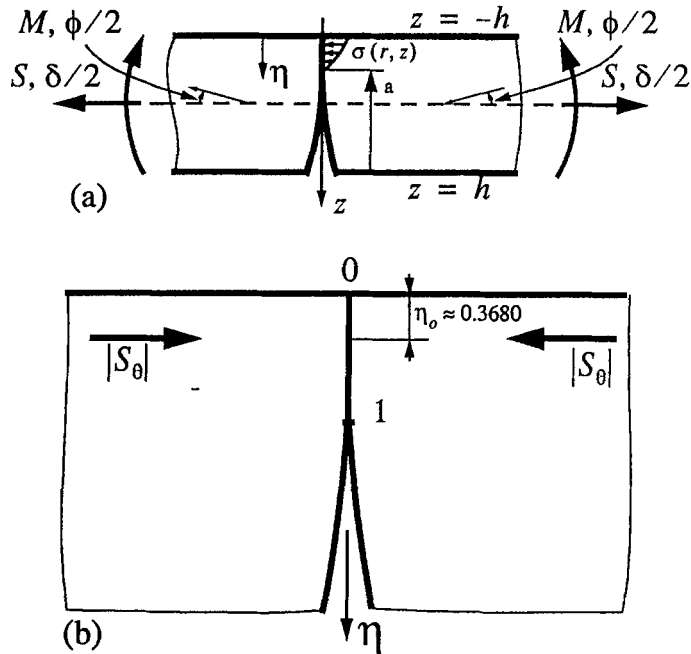
Fig. 5. (a) Edge-cracked strip under closure; (b) two elastic quarter planes under closure.

moment M per unit thickness proves crucial. The key issue in this paper is to unequivocally decide on the appropriate values of the global contact parameters e_f and e_c introduced earlier.

Following the procedure in [9], and given the configuration in Fig. 5a, it quickly follows that the mode I stress intensity factor is given by

$$K(a) = \sqrt{2h}(\sigma_s g_s + \sigma_m g_m), \tag{40}$$

where $\sigma_s = S/2h$ and $\sigma_m = 3M/2h^2$, while g_s and g_m are dimensionless functions of the crack depth to plate thickness ratio $\xi = a/2h$. In terms of the weight function approach employed by Wu and Carlsson [12] and the relevant expressions in Tada et al. [13], it follows that

$$g_s(\xi) = \sqrt{\pi\xi}\, f_s(\xi), \quad g_m(\xi) = \sqrt{\pi\xi}\, f_m(\xi), \tag{41}$$

in which

$$f_s(\xi) = \frac{F_s(\xi)}{(1-\xi)^{3/2}}, \qquad f_m(\xi) = \frac{F_m(\xi)}{(1-\xi)^{3/2}}. \tag{42}$$

In (42)

$$F_s(\xi) = \sum_{i=0}^{7} \alpha_i^s \xi^i, \qquad F_m(\xi) = \sum_{i=0}^{7} \alpha_i^m \xi^i. \tag{43}$$

The results presented in Table 3 of [14] apparently provide the most accurate normalized stress intensity factor and crack-mouth-opening displacement data for the tension and bending of an

Table 3. Edge-cracked strip SIF coefficients

i	α_i^s	α_i^m	i	α_i^s	α_i^m
0	1.1215	1.1215	4	27.437	34.836
1	−1.6109	−2.9725	5	−27.441	−35.100
2	6.9817	8.8068	6	15.252	19.489
3	−17.044	−21.257	7	−3.5748	−4.5500

edge-cracked strip, especially for long crack lengths ($\xi > 0.8$). A best fit of this SIF data leads directly to the following values for the coefficients α_i^s and α_i^m ($i = 0, 1, ..., 7$), consecutively, stated here in Table 3. The functions $F_s(\xi)$ and $F_m(\xi)$ are plotted in Fig. 6a.

In the calculations below, the behavior of various quantities will be required for long crack lengths or ξ large ($\xi \to 1$). The weight function approach employed in [12] is good even for long crack lengths, but still loses accuracy for $\xi > 0.85$. For this reason, the function g_m is obtained independently from [14].

Let δ and ϕ be the additional displacement and rotation of one end of the strip relative to the other due to the introduction of the crack. The latter quantities can be determined by equating the potential energy-release rate with the rate of change of compliance with crack length, as in [9]. Then

$$\delta = \frac{4h}{E'} \left(\alpha_{ss}\sigma_s + \alpha_{sm}\sigma_m \right),$$ (44)

$$\phi = \frac{12}{E'} \left(\alpha_{ms}\sigma_s + \alpha_{mm}\sigma_m \right),$$ (45)

in which, by elastic reciprocity, $\alpha_{sm} = \alpha_{ms}$. The $\alpha_{\lambda\mu}$ are dimensionless compliance coefficients and are defined by

$$\alpha_{\lambda\mu}(\xi) = \int_0^\xi g_\lambda(\xi')g_\mu(\xi')\,\mathrm{d}\xi'.$$ (46)

The closure contact widths central to this paper are achieved by first providing a wide-ranging ($0 \leqslant \xi = a/2h < 1$) description of the compliance coefficients, $\alpha_{\lambda\mu}$, as functions of the ratio $e_f = -M_\theta/S_\theta$. Similar to the approach used by Dempsey et al. [15], a wide-ranging (exact) description of the compliance coefficients, $\alpha_{\lambda\mu}$ is obtained by analytically integrating the expressions in (46); thus

$$\alpha_{\lambda\mu}(\xi) = \pi \sum_{k=0}^{14} g_k^{\lambda\mu}\gamma_k(\xi).$$ (47)

The compliance coefficients $g_k^{\lambda\mu}$ ($k = 1, 2, \ldots 14$) are presented in Table 4; the functions $\gamma_k(a)$ ($k = 1 \ldots 14$) in (47) are given by

$$\gamma_0(\xi) = \xi^2/2(1-\xi)^2,$$

Table 4. Compliance coefficients

k	g_k^{ss}	$g_k^{sm}=g_k^{ms}$	g_k^{mm}
0	1.2578	0.41922	0.13973
1	−0.56501	0.13227	0.15094
2	−0.45042	−0.31952	−0.081245
3	4.1169	3.3342	1.7156
4	−14.542	−10.985	−4.6772
5	26.931	19.333	6.4159
6	−21.479	−11.766	4.4499
7	−13.885	−25.429	−42.188
8	79.207	100.96	128.68
9	−170.83	−214.08	−268.30
10	253.08	317.04	397.18
11	−258.63	−324.87	−408.06
12	174.13	219.87	277.61
13	−69.863	−88.649	−112.49
14	12.779	16.265	20.703

$$\gamma_1(\xi) = \xi/(1-\xi) + \ln(1-\xi),$$
$$\gamma_2(\xi) = -\left(\xi + \ln(1-\xi)\right),$$
$$\gamma_k(\xi) = \left\{ \frac{[1-(1-\xi)^{k-2}]}{(k-2)} - \frac{[1-(1-\xi)^{k-2}]}{(k-2)} \right\}, \quad (k=3,4,\ldots 14). \tag{48}$$

Note that the general form for the first derivative of the compliances may be expressed in two forms, *viz.*,

$$\alpha'_{\lambda\mu}(\xi) = \frac{\pi\xi}{(1-\xi)^3} F_\lambda(\xi) F_\mu(\xi) = \frac{\pi\xi}{(1-\xi)^3} \sum_{k=0}^{14} g_k^{\lambda\mu}(1-\xi)^k. \tag{49}$$

An alternative form for the expressions in (47), useful for asymptotics and plotting purposes, is

$$\alpha_{\lambda\mu}(\xi) = \pi\xi^2 \Lambda_{\lambda\mu}(\xi)/(1-\xi)^2. \tag{50}$$

The compliance functions $\Lambda_{\lambda\mu}(\xi)$ are plotted in Fig. 6b. Note that

$$F_s(0) = F_m(0) = F_s(1) = 3F_m(1) \approx 1.1215$$

$$\Lambda_{ss}(1) = \Lambda_o \approx 0.6289, \quad \Lambda_{sm}(1) = \Lambda_{ms}(1) = \frac{\Lambda_o}{3}, \quad \Lambda_{mm}(1) = \frac{\Lambda_o}{9}. \tag{51}$$

Kinematic compatibility. The plate is considered to be rigid in the θ-direction; however, the circumferential displacement associated with the radial cracks requires further consideration. The procedure adopted here is to consider an element of a wedge sector of angle $\Delta\theta$. If
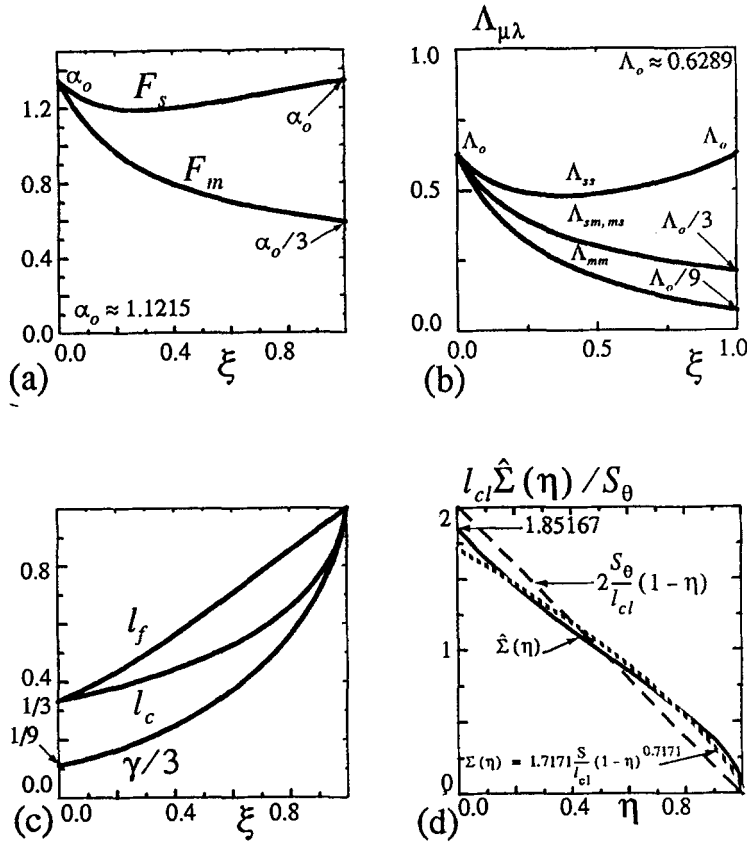
Fig. 6. (a) Stress intensity factor influence coefficients $F_s(\xi)$ and $F_m(\xi)$, (b) compliance coefficients $\Lambda_{\lambda\mu}(\xi)$, and (c) $\ell_f(\xi)$, $\ell_c(\xi)$ and $\gamma(\xi)/3$ plotted versus $\xi = a/2h$; (d) closure stress distributions (asymptotic approximation, accurate curve and wide-ranging approximation).

this element is subjected solely to a rigid body translation and rotation (unconstrained by the surrounding material), the wedge width $b_o(r, z)$, on noting (1), would be

$$b_o = (r - u_r)\Delta\theta = (r - u + zw')\Delta\theta. \tag{52}$$

The associated rotation of the element face in the θ-direction is given by

$$\alpha_o = \frac{\partial b_o}{\partial z} = w'\Delta\theta. \tag{53}$$

The additional rotation caused by the force S_θ and moment M_θ gives the combined rotation to be

$$\alpha = \left(\frac{w'}{r} - \frac{M_\theta - \nu M_r}{EI}\right) r\Delta\theta. \tag{54}$$

The kinematic closure constraint in (19) presumes that the plane $z = e_c$ within the radially cracked zone is a plane of zero strain. No interpenetration is allowed in the crack opening region (an obvious condition). That is, b_o in the crack opening region must not exceed the

width at $z = e_c$. In turn, this means that if $\alpha \neq 0$ then α must have the same sign as α_o. The following inequality is thus required to ensure non-negative crack opening displacements

$$\left(\frac{w'}{r} - \frac{M_\theta - \nu M_r}{EI} \right) \operatorname{sgn} w' \geqslant 0. \tag{55}$$

Radial cracking with closure. In this paper $M = -M_\theta = e_f S_\theta$ and $S = S_\theta$. Then, to simplify later analysis, let

$$\ell_f = -\frac{e_f}{h}, \quad \ell_c = -\frac{e_c}{h}, \quad \sum_m = \frac{\sigma_m}{\sigma_s} = -3\ell_f. \tag{56}$$

Each radial crack seeks its own natural extent of contact. Smooth crack-tip closure will then result such that

$$K(a) = 0 \quad \text{or} \quad \ell_f = \frac{1}{3} \frac{F_s(\xi)}{F_m(\xi)}. \tag{57}$$

In addition, given that the 'rigid plane' $z = e_c$ is required to be rigid, it is evident from (44), (45) and (50) that

$$\delta + e_c \phi = 0 \quad \text{or} \quad \ell_c = \frac{1}{3} \frac{\Lambda_{ss}(\xi) - 3\ell_f \Lambda_{sm}(\xi)}{\Lambda_{ms}(\xi) - 3\ell_f \Lambda_{mm}(\xi)}. \tag{58}$$

The value of ξ appearing in (58) is tied to the value of ℓ_f appearing in the same equation through (57). The functions ℓ_f and ℓ_c are plotted versus $\xi = a/2h$ in Fig. 6c.

Thus far, smooth closure of the crack faces has been assured by (57). Further, the rigidity or zero strain condition posed at $z = e_c$ has been stated in (58). The second and final kinematic condition requires rotational compatibility along the θ-lines bisecting each wedge sector formed by the n radial cracks. This, at first glance, would take the form

$$\phi + \alpha = 0 \quad \text{with} \quad \Delta\theta = 2\pi/n. \tag{59}$$

However, both ϕ in (45) and α in (54) are functions of r. Herein lies a weakness in the present formulation. In this paper, for simplicity and in order to obtain analytical results, the parameters e_f and e_c were chosen to be invariant with r, and functions solely of R (see (16)). There are many possible avenues at this juncture. While the formulation of the problem with variable e_f, e_c is a subject for a later study, the simplest step at this stage seems to be to take the average of (59)$_1$ in the form

$$\frac{1}{R} \int_0^R \phi(r)\, dr + \frac{1}{R} \int_0^R \alpha(r)\, dr = 0. \tag{60}$$

The latter condition simplifies to

$$\alpha_{ss} - 3\ell_f \alpha_{sm} + \frac{\pi \lambda}{(1+\nu)^2} \frac{\zeta}{\zeta^2 + b^2} = 0, \quad \lambda = \frac{R_o/h}{n}. \tag{61}$$
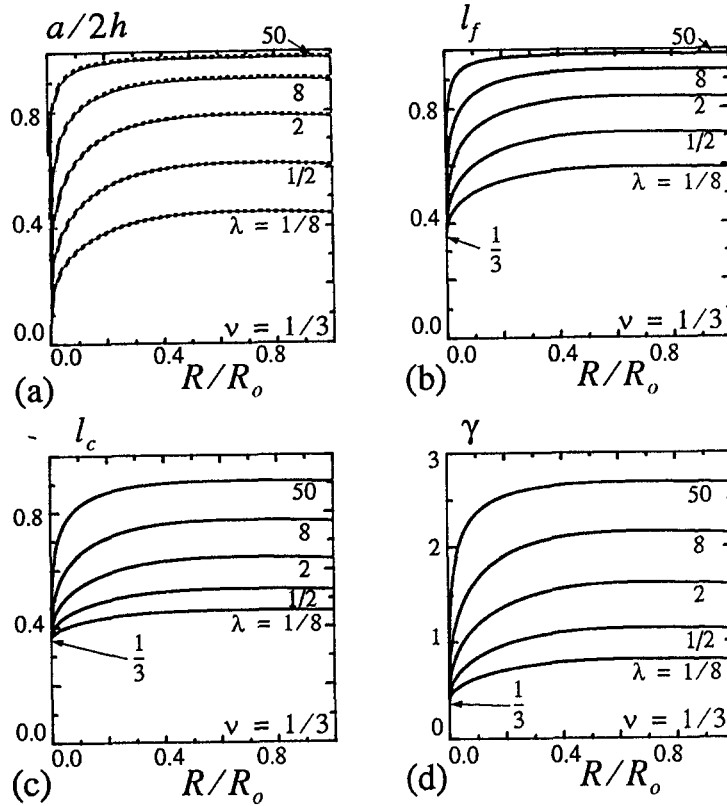
Fig. 7. (a) The through-the-thickness normalized crack length parameter $\xi = a/2h$, (b) $\ell_f(\xi)$, (c) $\ell_c(\xi)$, and (d) $\gamma(\xi)$ plotted versus R/R_o given various values of $\lambda \equiv R_o/nh$ and $\nu = 1/3$.

Asymptotic closure stress distribution. Consider the closure contact problem (Fig. 2c) under the force, S_θ, applied along the line of action $z = e_f < 0$. The stress distribution can be expressed as

$$\sigma(z) = f\left(\frac{2h}{2h-a}, \eta\right)\frac{S_\theta}{2h-a}, \quad \eta = \frac{h+z}{2h-a}. \tag{62}$$

In this qualitative expression, the crack depth a is defined by e_f. In terms of the η-coordinate, the extent of contact is invariable and remains equal to unity as $(z+h)/(2h-a)$ tends to the infinity under the condition $a \to 2h$. This limit corresponds to the contact of two elastic quarter-planes contacting along a zone of contact of unit length $0 \leqslant \eta < 1$ (Fig. 5b) under the force $S_\theta/(2h-a)$ applied at infinity along the line of action $z = e_f$. The asymptotic closure stress distribution is a function solely of η and directly proportional to S_θ/ℓ_{cl}, where $\ell_{cl} = 2h - a$. Such a contact problem is the same as the corresponding problem for an elastic half-plane with a semi-infinite crack perpendicular to the surface (with a zero stress intensity factor). Significantly, the desired closure contact stress is *unique* and valid in general under the condition $\ell_{cl} \ll 2h$.

As $a \to 2h$, and as h becomes very large (as for two quarter-planes), the parameter $\xi \to 1$. The 'outer' problem's closure parameters ℓ_f and ℓ_c both tend to unity (Fig. 6c). For the case of two contacting quarter planes, the 'inner' parameter, the difference between a and $2h$ has decreased to a finite constant value, here called the closure width, $\ell_{cl} = 2h - a$. The

line of action of the far-field force S_θ, denoted now by $\eta_o \ell_{cl}$ (Fig. 5b), has a unique value if $K(a) = 0$. This value is readily obtained from the paper by Kipnis [16] as

$$\eta_o = \frac{\pi/\sqrt{\pi^2 - 4}}{2\sqrt{2}G^-(1)} = 0.3680338,$$ (63)

in which $G^-(1) = 1.245698$. Referring again to the situation depicted in Fig. 5b (the unilateral contact of two quarter planes), note that η_o defines the line of action of the compressive forces $|S_\theta|$, with zero applied moment, such that $K(a) = 0$.

Suppose the closure stress distribution, in terms of η, is denoted by $\hat{\Sigma}(\eta)$ (as compared to $\sigma(z)$). A closed form solution to the closure stress distribution is available from the paper by Kipnis [16], who studied the symmetrical deformations of a semi-infinite crack lying on the bisector of an elastic wedge of angle 2α subjected to a far-field load and moment. For the case of $\alpha = \pi/2$ the eigenvalue equation in (1.4) of Kipnis gives $\lambda = n$ $(n = 1, 2, \ldots)$. Setting $K = 0$ to satisfy the closure condition, the accurate stress distribution $\hat{\Sigma}$ is found to be given by

$$\hat{\Sigma}(\eta) = \frac{S_\theta}{\ell_{cl}} \sqrt{\frac{2\pi}{\pi^2 - 4}}$$

$$\times \left(\frac{8/\pi\sqrt{\pi}}{G^+(-1)} - \sum_{n=2}^\infty \frac{2n^2 - 1 + \cos(n\pi)}{n\pi(n-1)\cos(n\pi)} \frac{\Gamma(1+n)}{\Gamma(\frac{1}{2}+n)} \frac{\eta^{n-1}}{G^+(-n)} \right),$$ (64)

in which

$$G^\pm(x) = \exp\left\{ \pm \frac{|x|}{\pi} \int_0^\infty \frac{\ln g(\xi)}{\xi^2 + x^2} \, d\xi \right\}.$$ (65)

In (65),

$$g(x) = \frac{\cosh(2\pi x) - 2(1 + 2x^2)\cosh(\pi x) + 1}{\cosh(2\pi x) - 1}.$$ (66)

The function $g(0) = (\pi^2 - 4)/2\pi^2$, while $g(x)$ rapidly tends to unity for large x. The accurate closure stress distribution in (??) and the approximate expression in (67) are plotted in Fig. 6d. Note that the accurate value for the maximum stress is only slightly modified from the approximate value in (67)$_2$: $\sigma_{max} \approx 1.85 S/\ell_{cl}$.

This closure stress is well approximated by the simple expression $\Sigma = \Sigma_o(1 - \eta)^p$; for this distribution, the average value $(\Sigma_o/(p + 1))$ acts at $\eta_o = 1/(p + 2)$. From (63), $p = 0.7171$ and then

$$\Sigma(\eta) \approx 1.7171(S_\theta/\ell_{cl})(1 - \eta)^{0.7171}, \quad \sigma_{max} \approx 1.85 S_\theta/\ell_{cl}.$$ (67)

The maximum contact stress, which is especially important with regard to crushing considerations, is defined as well.
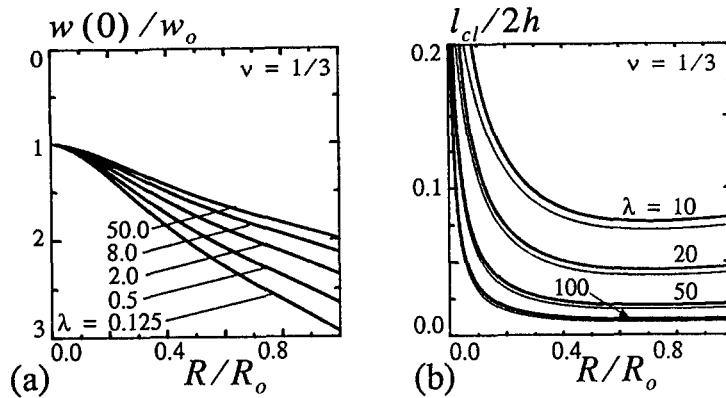
Fig. 8. (a) The central plate deflection versus R/R_o, and (b) the closure width $\ell_{cl}/2h$ (exact: thick solid line; approximate–see (98): thin solid line), given various values of λ and $\nu = 1/3$.

An alternative deduction of the value of η_o is as follows. First, the behavior of e_f as $a \to 2h$ needs to be determined. Remembering that $\ell_f = -e_f/h$, note that for $\xi = 1 - \epsilon$ and $\epsilon \to 0$

$$\ell_f \sim 1 - k_f \epsilon, \quad k_f = \frac{d\ell_f}{d\xi}(1) \tag{68}$$

Recalling that $\ell_f(1) = 1$, k_f can be defined as $\ell'_f(1)/\ell_f(1)$, or, equivalently, as

$$k_f = \hat{F}_s(1) - \hat{F}_m(1), \quad \hat{F}_\mu = \frac{1}{F_\mu(1)}\frac{dF_\mu}{d\xi}(1) \tag{69}$$

From (68), $h + e_f \sim (1/2)k_f \ell_{cl}$. Given that $\eta_o \equiv (h + e_f)/\ell_{cl}$, it quickly follows that $\eta_o = k_f/2$. However, the curve fit expressions in (43) and Table 3 would give an inaccurate value of 0.3824 for η_o. A more precise curve fitting of the original data from [14] using Tablecurve [17] (an automated nonlinear curve fitting program that uses a 64-bit Levenburg-Marquardt algorithm) was attempted. The best-fit was obtained using a rational function of two fourth order polynomials and gave a value of 0.3687. The interesting point here is that an extra constraint on the functions $F_s(\xi)$ and $F_m(\xi)$ is now available via (69); that is,

$$k_f = \hat{F}_s(1) - \hat{F}_m(1) = 2\eta_o = 0.7360675. \tag{70}$$

The values listed in Table 3 are quite adequate unless rather special asymptotic considerations are involved, as above.

A simple, rather general, approximation for the closure stress distribution, applicable for arbitrary values of the closure width ℓ_{cl}, is

$$\Sigma(\eta) = 2(S_\theta/\ell_{cl})(1 - \eta). \tag{71}$$

Asymptotic behavior. Further simplifications follow if the behavior of the compliance coefficients $\alpha_{\lambda\mu}$ in (50) is determined for $\xi \to 1$. Therefore, again let $\xi = 1 - \epsilon$ and $\epsilon \to 0$

$$\alpha_{\lambda\mu} \sim \frac{\pi}{(1 - \xi)^2}\Lambda_{\lambda\mu}(1)(1 - 2\epsilon - k_{\lambda\mu}\epsilon), \quad k_{\lambda\mu} = \frac{1}{\Lambda_{\lambda\mu}(1)}\frac{d\Lambda_{\lambda\mu}}{d\xi}(1). \tag{72}$$

Further, note (69) and the following identities

$$\Lambda_{\lambda\mu}(1) = F_\mu(1)F_\lambda(1)/2, \quad k_{\lambda\mu} = 2\hat{F}_\mu + 2\hat{F}_\lambda,$$

$$2k_f = k_{ss} - k_{sm} = k_{ms} - k_{mm}, \quad \text{and} \quad k_{ss} + k_{mm} = 2k_{sm}. \tag{73}$$

The latter identities provide that, for $\xi \to 1$,

$$\alpha_{ss} - 3\ell_f\alpha_{sm} \sim -\frac{\pi\Lambda_o k_f}{(1-\xi)}, \quad \alpha_{ms} - 3\ell_f\alpha_{mm} \sim -\frac{\pi\Lambda_o k_f}{3(1-\xi)}. \tag{74}$$

Using (74), as well as (44) and (45),

$$\delta \sim -\frac{2\pi\Lambda_o k_f}{E'(1-\xi)}S_\theta, \quad \phi \sim -\frac{2\pi\Lambda_o k_f}{E'h(1-\xi)}S_\theta. \tag{75}$$

The latter equation reveals that the $\phi \sim \delta/h$ as $\xi \to 1$. This result corresponds to straight crack surfaces which are normal to the plate neutral axis and plate surfaces over almost the entire plate thickness. Thus, at each radial crack line, the plate presumes that there is merely line contact at $z = -h$. This phenomenon can be explained by considering the inner elasticity solution and the asymptotic closure stress distribution.

6. An approximate solution for $\xi(\lambda, \zeta, \nu)$

Equation (61) harbors the influences of the normalized radius ($\zeta = R/R_o$) of the radially cracked zone, the parameter $\lambda = R_o/nh$, and Poisson's ratio on $\xi \equiv a/2h$. Once ξ is known, ℓ_f, ℓ_c, γ and, as it turns out, all aspects of the solution are known. For this reason, some effort was devoted to obtaining an accurate pseudo-analytical solution to ξ in (61) in terms of ζ, λ and ν.

An accurate approximation to $\alpha_{ss} - 3\ell_f\alpha_{sm}$ is found to be given by, noting (50),

$$\Lambda_{ss} - 3\ell_f\Lambda_{sm} = -a_o\left((1 + 4\vartheta)\xi(1 - \xi) - \xi(1 - \xi)^2\right), \tag{76}$$

in which $a_o = 0.1345$ and $\vartheta = 0.44475$. This approximation produces the following quartic:

$$\xi^4 + 4\vartheta\xi^3 + \chi\xi - \chi = 0, \tag{77}$$

in which

$$\chi = \frac{\lambda}{a_o(1 + \nu)^2}\frac{\zeta}{\zeta^2 + b^2}. \tag{78}$$

Equation (77) has the resolvent cubic equation

$$\varrho^3 + p\varrho + q = 0, \tag{79}$$

in which $p = 4(1 + \vartheta)\chi$ and $q = 16\vartheta^2\chi - \chi^2$. The latter equation has the solution

$$\varrho = (\delta - q/2)^{1/3} - (\delta + q/2)^{1/3}, \tag{80}$$

where $\delta = ((p/3)^3 + (q/2)^2)^{1/2}$. The solution for ξ is now given by

$$\xi = \frac{1}{2}\left(\frac{\chi + 8\vartheta^3}{\sqrt{\vartheta^2 + \varrho/4}} + 8\vartheta^2 - \varrho\right)^{1/2} - (\vartheta^2 + \varrho/4)^{1/2} - \vartheta. \tag{81}$$

The remarkable accuracy of the solution for $\xi = a/2h$ presented in (81) is quickly evident from Fig. 7a: the numerical solution of (61) versus (81) is plotted versus R/R_o for various values of λ, given $\nu = 1/3$. The approximate solution is clearly very accurate. The associated plots of ℓ_f, ℓ_c and γ versus $\zeta = R/R_o$ are presented in Figs. 7b-7d, respectively.

7. Energy balance and fracture criterion

The remaining task of this paper is to explore the energy release rate G as a function of the degree of closure and radially cracked zone radius. While the global expression for G is readily stated, the expression obtained from local considerations is not so readily obtained. In fact, the latter form for G is rather special and does not appear to have been derived previously for a problem of this type.

The loss in potential energy due to the growth of the system of radial cracks from the length R to $R + \Delta r$ is deduced by considering the annulus so-formed. The change in potential energy $\Delta\Pi$ is given by

$$\Delta\Pi = \Delta U - \Delta W, \tag{82}$$

in which the ΔU is the increase in strain energy and ΔW is the difference between the work done by S_r, M_r, and Q_r at the $R + \Delta r$ and R boundaries of the annulus.

Note that work is done only by the load quantities acting on circumferential boundaries. The quasi-continuum axisymmetric approach adopted in this paper presupposes a 'large enough' number of cracks. This continuous model is an asymptotic approximation of the radially cracked plate, as the number (n) of cracks grows large. Naturally, a symmetrical layout of these n radial cracks is assumed. Moreover, the external loading as well as the boundary conditions (7) give us a symmetrical problem in the sense that the deformations of the plate considered are symmetrical with respect to any crack line. For instance, consider a plate element bordered by $r = R + \Delta r$, $r = R$, and by the rays $\theta = \theta_j$ and $\theta = \theta_{j+1}$. Let these rays be neighboring cracks; each crack or ray are axes of symmetry, because

$$w(\theta - \theta_j) = w(\theta_j - \theta), \quad w(\theta - \theta_{j+1}) = w(\theta_{j+1} - \theta), \tag{83}$$

with similar expressions for u_r, S_r, M_r, Q_r, S_θ and M_θ. Because of the above-mentioned symmetry, the boundaries $\theta = \theta_j$ and $\theta = \theta_{j+1}$ manifest themselves as rigid, smooth lines. The force S_θ as well as the moment M_θ do act on contiguous plate elements but do no work because the lines are rigid.

Given linear elastic deformations only, the accumulated strain energy in the annulus $r - \Delta r/2 < r < r + \Delta r/2$ is contributed via the work of S_r, M_r and Q_r which act at $r \pm \Delta r/2$, and an external distributed normal loading $q_z(r)$. Thus,

$$A(r) = \pi\left(r(S_r u + Q_r w + M_r w')r\right)' + \pi r q_z w, \tag{84}$$

$2\pi(1+\gamma)\,[M_\theta]\,/P$

$l_{cl}/2h$

$nGEh^4/P^2R_o$
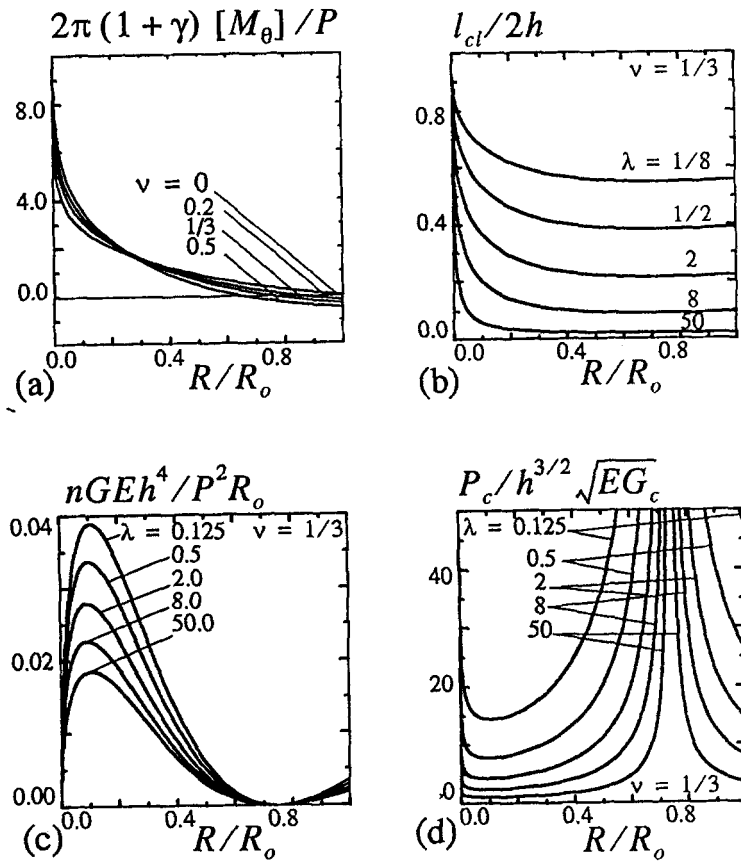
$P_c/h^{3/2}\sqrt{EG_c}$

Fig. 9. (a) Jump in the tangential bending moment $[M_\theta(R)]$, (b) closure width $\ell_{cl}/2h \equiv (2h - a)/2h$, (c) total energy release rate, and (d) load bearing capacity versus $\zeta = R/R_o$ given various values of $\lambda \equiv R_o/nh$ and $\nu = 1/3$.

in which $A(r)$ denotes the strain energy per unit radial length, hereafter called the strain energy density.

The change in strain energy due to the growth of the system of radial cracks from the length R to $R + \Delta r$ can now be calculated. The limit as $\Delta r \to 0$ is discussed. Let the subscript '$-$' correspond to the crack region $r = R - 0$, and the subscript '$+$' correspond to the intact region $r = R + 0$ (before the variation). Taking into account the continuity conditions at the boundary (26), one can express the difference required as

$$A_- - A_+ = \pi R \left\{ (S_r u + Q_r w + M_r w')'_{R-} \right.$$
$$\left. -(S_r u + Q_r w + M_r w')'_{R+} \right\}. \tag{85}$$

With the notation defined in (26), (85) can be rewritten as

$$[A] = \pi R \left(S_r[u'] + M_r[w''] + u[S'_r] + w'[M'_r] \right)_R. \tag{86}$$

Note from (85) and (86) that the increase in strain energy is given by

$$\Delta U = -[A]\Delta r. \tag{87}$$

ΔW is the difference between the work done by S_r, M_r and Q_r on the boundaries of the annulus defined by $r = R + \Delta r$ and $r = R$:

$$
\begin{aligned}
\Delta W &= 2\pi R \left\{ (M_r \delta w' + S_r \delta u + Q_r \delta w)_{R+\Delta r} \right. \\
&\quad \left. - (M_r \delta w' + S_r \delta u + Q_r \delta w)_R \right\}.
\end{aligned}
\tag{88}
$$

Noting that

$$
\delta w'|_{R+\Delta r} - \delta w'|_R = \left(w''_- - w''_+ \right) \Delta r,
\tag{89}
$$

with similar relationships for the other variations, the expression in (88) becomes

$$
\Delta W = -2\pi R \left\{ M_r [w''] + S_r [u'] \right\}_R \Delta r.
\tag{90}
$$

The loss in potential energy is now expressible in concise form; taking note of (82), (87), (86), (28),

$$
\begin{aligned}
\Delta \Pi = -\pi R \left\{ \left(\frac{\nu}{2Eh} S_r + \frac{u}{R} \right)_{R+} [S_\theta] \right. \\
\left. + \left(\frac{\nu}{EI} M_r + \frac{w'}{R} \right)_{R+} [M_\theta] \right\} \Delta r.
\end{aligned}
\tag{91}
$$

To simplify (91) note from (6d) and from (6b) jointly with (4a) that in the intact region

$$
\frac{S_\theta}{2Eh} = \frac{\nu S_r}{2Eh} + \frac{u}{r}, \quad \frac{M_\theta}{EI} = \frac{\nu M_r}{EI} + \frac{w'}{r}, \quad (R < r \leqslant R_o).
\tag{92}
$$

Now let G denote the energy-release-rate per crack in the radially cracked zone; presuming the formation or existence of n cracks, it follows from (91) that

$$
nG = \frac{\pi R}{2h} \left\{ \frac{[S_\theta]}{2Eh} S_\theta(R^+) + \frac{[M_\theta]}{EI} M_\theta(R^+) \right\} \quad \text{(closure − intact)}.
\tag{93}
$$

Significantly, the above expression differs fundamentally from that in [8]. It is important to note here that (93) has been derived without specifying any relationship between S_θ and M_θ; the closure conditions in (29) have not yet been utilized.

If crack closure is ignored for the whole inner region $(0 \leqslant r \leqslant R)$, $[S_\theta] = 0$, $M_\theta(R^+) = [M_\theta]$ and

$$
nG = \frac{\pi R}{2h} \frac{[M_\theta]^2}{EI} \quad \text{(open − intact)}.
\tag{94}
$$

Local energy balance.   Equations (92) and (19) provide that $[S_\theta]/2Eh = e_c[M_\theta]/EI$ (another form of (29)); by subtracting $M_\theta(R^-) + e_f S_\theta(R^-) = 0$ (from (18)) the local energy-release-rate expression in (93) becomes

$$
nG_{\text{local}} = \frac{\pi R}{2h} \left\{ (1 + \gamma) \frac{[M_\theta]^2}{EI} + (e_c - e_f) \frac{[M_\theta]}{EI} S_\theta(R^+) \right\}.
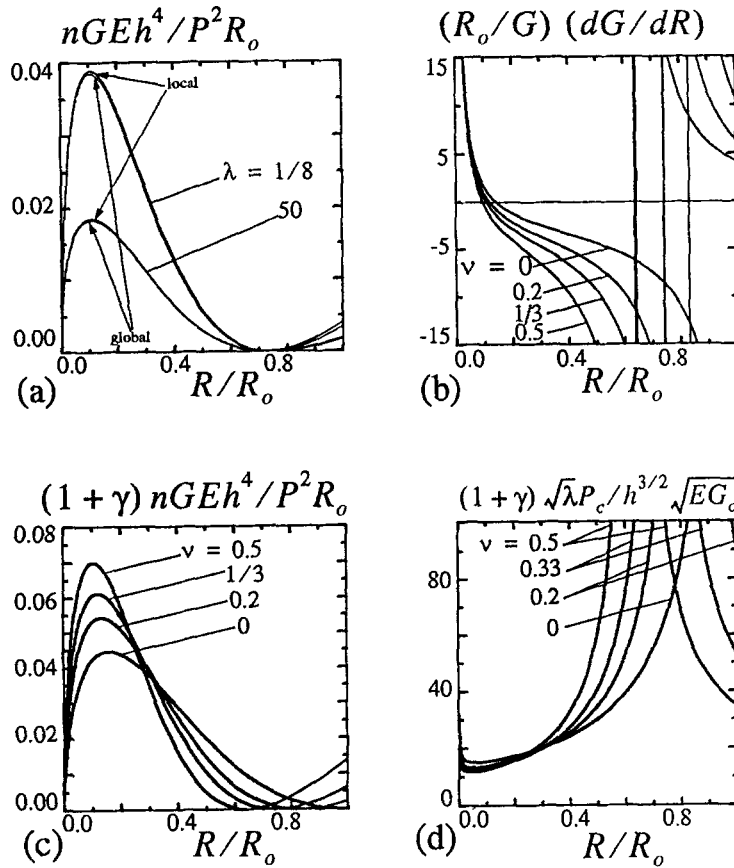\tag{95}
$$

Fig. 10. (a) Comparison of the local and global total energy release rates ($\nu = 1/3$), (b) geometric stability factor $(R_o/G)(\mathrm{d}G/\mathrm{d}R)$, and normalized (c) energy-release-rate G and (d) critical load P_c plotted versus R/R_o for various values of Poisson's ratio, ν.

For the clamped circular plate problem treated in this paper, it follows from (32) and (34) that

$$
[M_\theta] = \frac{P}{4\pi} \left\{ \frac{1+\nu}{1+\gamma} - \frac{2b^2[1-(1+\nu)\ln\zeta]}{(1+\gamma)(\zeta^2+b^2)} \right\},
$$

$$
S_\theta(R^+) = \frac{\gamma}{e_f} \frac{P}{4\pi} \frac{[1-(1+\nu)\ln\zeta]}{(1+\gamma)} \frac{\zeta^2-b^2}{\zeta^2+b^2}.
$$

(96)

Global energy balance. The global energy-release-rate expression takes the form

$$
nG_{\text{global}} = \frac{1}{2}\frac{P}{2h}\frac{\partial w(0)}{\partial R} + \pi \int_0^{R_o} q_z(r')\frac{\partial w}{\partial R}(r')r' \, \mathrm{d}r'.
$$

(97)

The local and global energy-release-rate expressions stated in (93) and (97), respectively, must be equivalent.

The central displacement $w(0)$ stated in (35) is a function of R explicitly *and* implicitly via γ (note (16) and (21)). If this fact were overlooked, the global energy-release-rate expression in (97) would be found to give only the first term in (95).

8. Results

The central deflection $w(0)$ (35), normalized by w_o (11), is plotted in Fig. 8a versus the normalized crack length R/R_o, for various values of $\lambda = R_o/nh$ and $\nu = 1/3$. With $\gamma = 3\ell_c\ell_f$, the dependence of γ on R must be deduced via (57), (58), and either (61) or (81). One can interpret Fig. 8a to note that the greater the number of cracks, the greater the central deflection. Of course, the greater the radius R, the greater the central deflection.

There is a distinct dependence on the radius of the radially cracked zone R and the number of cracks n. Note from Fig. 8b (or Fig. 9b) that increasing closure widths are associated with an increase in the number of cracks; the latter increase lowers the value of λ. To examine this further, the quartic in (77) was recast in terms of $(1 - \xi)$ and higher order terms were neglected. The resulting expression predicted that the asymptotic closure width for $a \to 2h$ (for large values of λ) behaves as

$$\frac{\ell_{cl}}{2h} = \frac{1 + 4\vartheta}{4 + 12\vartheta + \chi}. \tag{98}$$

The expression in (98) is accurate for $\lambda \geqslant 10$ (Fig. 8b). Clearly, if ℓ_{cl} is to tend to zero, λ must tend to very large numbers. This implies that the magnitude of R_o/h be very large; this in turn implies that very long crack lengths are required to have $\ell_f \to 1$ (see Fig. 6c). Apparently, Hellan's analysis [8] (who assumed $e_f = e_c = -h$, which in turn implies that $\ell_f = \ell_c = 1$) is valid only for very long cracks.

In Fig. 9a, the plot of the jump in the tangential bending moment $[M_\theta(R)]$ reveals the zeros already stated in Table 2. This plot applies equally well to open-intact (with $\gamma = 0$) as to closure-intact. In Fig. 9b, the numerical solution of (61) gives the closure width $\ell_{cl}/2h \equiv (2h - a)/2h$ versus $\zeta = R/R_o$ given various values of $\lambda \equiv R_o/nh$ and $\nu = 1/3$. These two plots are remarkably informative. Remember that ℓ_f and ℓ_c are specified to be constant for a particular radius R. Figure 7b now gives the necessary value of ℓ_f for any ζ, given ν and λ. Now one can readily reason that the fewer the number of cracks, the higher the value of ℓ_f, or, conversely, the smaller the value of the closure contact width ℓ_{cl}. Note that $\ell_f \to 1$ only for very high values of λ. Alternatively, the greater the number of cracks, the greater the magnitude of the closure width (Fig. 9b).

The plots in Figs. 9c and 9d portray the normalized total energy release rate and the critical load, respectively. The unbounded behavior in the plot of the critical load (Fig. 9d) is directly associated with the zero energy release rate in Fig. 9c. A radius R_c (see Table 2) at which $G = 0$ imposes an insurmountable barrier to crack propagation, as revealed by the critical loads tending to 'infinity' for various values of $\lambda = R_o/nh$ in Fig. 9d. Note in Fig. 9d that radially cracked zones smaller than a certain critical radius (hereafter called r_c) will propagate unstably. This extent of instability extends over increasingly larger distances, the higher the value of λ (and, qualitatively, the fewer the number of cracks). If the pre-existing cracked zone radius is greater than r_c, stable crack growth will be encountered at the outset. Eventually, however, crack growth stability will be experienced, and for relatively short crack lengths (compared to the plate diameter). At this stage, crack propagation will require an associated monotonic increase in load. The load will increase until circumferential failure occurs.

The unbounded behavior evident for very short crack lengths in Fig. 9d is indicative of the behavior discussed earlier in the paper in the section on localized loading. Regardless, radial cracking within a very small radius is patently unrealistic. Actually, considerations of surface cracks and slanted crack fronts are clearly involved.

Figures 9c and 9d reveal that the total energy release rate and critical load are significantly influenced by the value of λ; for a fixed value of R_o/h, λ is proportional to $1/n$. Figure 9c then says that the total energy release rate increases with the number of cracks (which is clearly expected) while Fig. 9d says that the load bearing capacity increases as the number of cracks increases. Once again, the load limiting mechanism will be sequential circumferential cracking often followed by penetration due to shear. Although it is not obvious, λ typically varies little in any specific practical scenario; here, the range between two adjacent curves in Fig. 9c is implied. In this case, the conclusion put forward in the section entitled 'Few' versus 'Many' cracks, is found to be true.

A comprehensive study of the energy expressions are portrayed in Fig. 10. The global energy release rate expression presented in (97) is compared with the local expression (95) in Fig. 10a for two values of λ. The plot in Fig. 10a is very important: the global vs local agreement serves to confirm that the present paper is correct in its formulation, kinematic assumptions, and development. Furthermore, the validity of the local energy release rate expression stated in (95) is also confirmed.

The function $(R_o/G)(dG/dR)$ plotted versus R/R_o in Fig. 10b is a widely used crack growth stability indicator [18, 19]. Interestingly, Fig. 10b reveals that the crack growth stability behavior is not influenced by closure effects. The normalized plots in Figs. 10c and 10d portray the significant dependence on Poisson's ratio.

9. Discussion and conclusions

The crack closure phenomena treated in this paper provide a framework for the application of fracture mechanics to cracked plates subjected to closure. Crack closure exerts a major influence on the compliance of cracked plates under bending, and the different types of (complex) crack systems formed under different loading conditions. As a result, crack closure is a key ingredient in applications involving the quasi-static and dynamic forcing of cracked plates. The asymptotic distributions of the closure contact width and the closure stresses are applicable to even rather short cracks of rather general shape as well as to general systems of cracks. In the dynamics of a plate subjected to crack closure, in particular, the mechanics of wave propagation and reflection have yet to be considered. Finally, the fracture mechanics presented in this paper can be used to analyze the stability of compression loaded symmetrically cracked configurations undergoing crack closure.

The quasi-continuum formulation of this paper presupposes complete symmetry with respect to the crack lines and there is the distinct possibility that this is not a stable state. If there is a mismatch in deflection from one sector to another, it is natural to enquire what is the stable state. The importance of this question increases with the crack length since the width of the closure strip decreases. Detailed considerations of this problem lead to a geometrically nonlinear contact problem and is outside the scope of this paper. This paper has also presupposed the symmetric *growth* of a system of radial cracks of *equal* length. The stability aspects related to these assumptions are to be explored in the near future.

The main conclusions of this paper are as follows:

1. The quasi-continuum 'many crack' problem solution has been derived for a nonzero closure contact width. The bearing capacity of such a cracked plate has been determined. The larger the number of cracks, the greater the bearing capacity.
2. A local and global expression for the energy release rate has been determined.

3. An accurate evaluation and approximate expression for the asymptotic closure contact stress distribution has been obtained and plotted; an approximate distribution valid for arbitrarily large closure widths has been stated.
4. The asymptotic closure stress distribution is unique and universal. The generality of the local plane contact conditions forms the basis for this universality. This result is valid both for any through-the-thickness crack, including a curvilinear crack and for more general crack systems.
5. The limiting crack zone size (compared to the plate radius) depends significantly on Poisson's ratio.
6. The total energy release rate is dependent on crack length, Poisson's ratio and the number of cracks. The fewer the number of cracks, the smaller the closure contact width. Correspondingly, the larger the number of cracks, the greater the closure width.
7. The crack growth stability characteristics are not influenced by crack closure; the load bearing capacity and central deflection, on the other hand, are significantly influenced by crack closure. After crack initiation, which is expected to be unstable, it is clear that considerable resistance to further crack growth will be observed. For a material like ice, it is highly likely that sequentially smaller crack jumps occur prior to eventual breakthrough.

Acknowledgements

References

1. J.P. Dempsey and Z.G. Zhao, *Journal of the Mechanics and Physics of Solids* 41 (1993) 487–506.
2. D.S. Sodhi, *ASCE Journal of Cold Regions Engineering* 9 (1995) 4–22.
3. D.S. Sodhi, *Ice Mechanics – 1995*, J.P. Dempsey and Y.S. Rajapakse (eds.), ASME AMD.
4. L.I. Slepyan, *Mechanics of Solids* (translation of *Izvestiya AN SSSR: Mekhanika Tverdoga Tela*) 25 (1990) 155–161.
5. Y.N. Li and Z.P. Bazant, *ASCE Journal of Engineering Mechanics* 120 (1994) 1481–1498.
6. D.P. Jones and J.L. Swedlow, *International Journal of Fracture* 11 (1975) 897–914.
7. F.S. Heming, *International Journal of Fracture* 16 (1980) 289–304.
8. K. Hellan, *International Journal of Fracture* 26 (1984) 17–30.
9. J.R. Rice and N. Levy, *Journal of Applied Mechanics* 39 (1972) 185–194.
10. J. Dundurs, in *Mechanics of Contact between Deformable Bodies*, A.D. de Pater and J.J. Kalker (eds.) Delft University Press (1975) 54–66.
11. S. Timoshenko and S. Woinowsky-Krieger, in *Theory of Plates and Shells*, Second edn., McGraw-Hill (1959).
12. X.-R. Wu and A.J. Carlsson, *Weight Functions and Stress Intensity Factor Solutions*, Pergamon Press (1991).
13. H. Tada, P.C. Paris, and G.R. Irwin, *The Stress Analysis of Cracks Handbook*. Del Research Group, St. Louis, (1985).
14. A.C. Kaya and F. Erdogan, *Quarterly of Applied Mathematics* 45 (1987) 105–122.
15. J.P. Dempsey, R.M. Adamson and S.J. DeFranco, *International Journal of Fracture* 69 (1995) 281–294.
16. L.A. Kipnis, *Journal of Applied Mathematics and Mechanics* (translation of PMM) 43 (1979) 164–170.
17. TableCurve, Jandel Scientific, San Rafael, CA (1992).
18. C. Gurney and J. Hunt, *Proceedings of the Royal Society* A361 (1967) 254–263.
19. S.J. DeFranco and J.P. Dempsey, *Journal of Glaciology* 40 (1994) 451–462.